Spectral and temporal dynamics of nonequilibrium phonons in $LaF_3:Pr^{3+}$

W. A. Tolbert,* W. M. Dennis, and W. M. Yen
Department of Physics and Astronomy, University of Georgia, Athens, Georgia 30602
(Received 4 March 1991)

Defect-induced one-phonon absorption is used to generate high-occupation-number narrow-band nonequilibrium phonon populations at a range of frequencies in $LaF_3:Pr^{3+}$. The spectral and temporal dynamics associated with the return to equilibrium of these phonons is observed. Processes that dominate the spectral evolution are shown to be narrow-band phonon confluence, anharmonic decay, and the broadband confluence of anharmonic decay products. The experimental data are shown to be in good agreement with a phonon-occupation-number rate-equation analysis that incudes the above processes.

INTRODUCTION

The mechanisms by which a narrow-band nonequilibrium phonon population decays and evolves to a new equilibrium has been the subject of a large body of both experimental and theoretical work.[1] To our knowledge the spectral evolution of an initially narrow-band phonon distribution to the establishment of a new thermal distribution has not been observed in its entirety, as the detailed observation of phonon relaxation processes requires the combination of a narrow-band tunable source of bulk phonons and a frequency-selective detection scheme. In a recent work[2] we have demonstrated that defect-induced one-phonon absorption (DIOPA) of far-infrared radiation (FIR) can be used to generate highly monochromatic nonequilibrium phonon populations with occupation numbers greater than one, at a range of frequencies throughout the Brillouin zone in $LaF_3:Pr^{3+}$. This generation mechanism relies on the presence of lattice defects to relax k conservation, enabling acoustic phonons of frequency ν_g to be generated directly by light of frequency ν_g.[3] In this paper we utilize DIOPA in conjunction with anti-Stokes absorption vibronic sideband spectroscopy[4,5] to investigate with both spectral and temporal resolution the dynamics associated with the return to equilibrium of monochromatic phonon distributions in LaF_3. We believe that this is the first direct observation of the phenomenon for bulk phonons. The dynamic behavior of these phonons is modeled using a set of rate equations which take into account the interactions of both narrow- and broadband phonon distributions.

EXPERIMENTAL

Phonons are generated using defect-induced one-phonon absorption of far-infrared radiation in the frequency range of 25 to 70 cm^{-1}, with the complete spectral evolution being obtained for phonons generated at 34.7 and 51.9 cm^{-1}. Spectrally and temporally resolved phonon detection is achieved through the use of anti-Stokes absorption vibronic sideband spectroscopy. A schematic of this technique as implemented in $LaF_3:Pr^{3+}$ is shown in Fig. 1. An optical pulse incident on the sample at a frequency Δ less than the zero phonon line is transmitted through the sample without absorption in the absence of phonons. In the presence of phonons of frequency Δ, absorption to the $^3P_0$ takes place and fluorescence to the $^3H_6$ ensures. A zero-background measurement of the phonon-induced absorption can be obtained by monitoring the time-integrated fluorescence to the $^3H_6$.

The absorption coefficients for the Stokes and anti-Stokes sidebands are given by

$$\alpha_S(\varepsilon_0+\Delta)=C[n(\Delta)+1]\sum_\lambda \rho(\Delta,\lambda)F(\Delta,\lambda) \tag{1a}$$

and

$$\alpha_{AS}(\varepsilon_0-\Delta)=Cn(\Delta)\sum_\lambda \rho(\Delta,\lambda)F(\Delta,\lambda)\,, \tag{1b}$$

where ε_0 and Δ are the frequency of and the detuning from the zero-phonon transition, respectively. $\rho(\Delta,\lambda)$ and $F(\Delta,\lambda)$ are the phonon density of states and

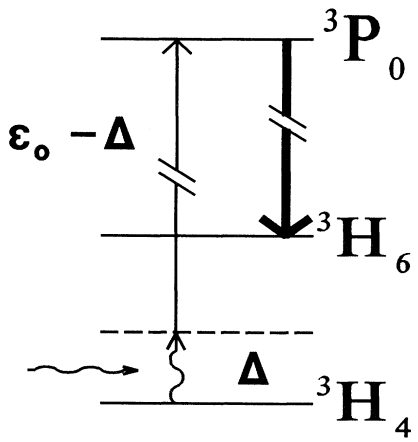

FIG. 1. Energy level diagram of $LaF_3:Pr^{3+}$ showing the states utilized for the anti-Stokes absorption vibronic sideband spectrometer. ε_0 is the $^3H_4$-$^3P_0$ energy and Δ is the detuning of the probe laser from ε_0, i.e., the phonon energy.

electron-phonon coupling for phonons of frequency Δ and branch λ, and C is a constant. The phonon occupation number can be calculated from

$$n(\Delta)=\frac{\alpha_{AS}(\varepsilon_0-\Delta)}{\alpha_S(\varepsilon_0+\Delta)} \quad (2)$$

if $\alpha_S(\varepsilon_0+\Delta)$ is measured at low temperature and in the absence of nonequilibrium phonon generation. It should be noted that absorption from phonon populated Stark split components of the ground state has a higher cross section than absorption from the phonon sideband. This causes regions of increased sensitivity in the phonon spectra which cannot be removed by normalization, hence the phonon spectra cannot be accurately measured close to these electronic states.

Phonon transients are obtained by monitoring the time-integrated fluorescence as a function of the delay between the FIR phonon generation pulse and the optical detection pulse. Time-resolved phonon spectra are constructed from a series of transients at different detunings Δ. The temporal resolution of this technique is determined by the convolution of the FIR and visible laser pulse widths. The spectral resolution is limited by the convolution of the dye laser frequency and the $^3P_0$ linewidth (0.53 cm^{-1}).[6] It should be noted that this technique detects only those phonons which are present during the optical pulse and hence is not sensitive to any phonons that may be generated by nonradiative decay during the optical detection process.

The experimental setup for these experiments is depicted in Fig. 2. Far-infrared radiation is obtained by using a transversely excited atmospheric CO_2 laser to pump a 6-m superadiant cell.[7] FIR pulse energies of >1 mJ can be obtained for over 30 lines in the region 20–100 cm^{-1}. The bandwidth of the FIR pulses was measured using an FIR Fabry-Perot interferometer to be less 500 MHz. The FIR pulse width was determined to be <50 ns using a 100-ps-response pyroelectric detector.

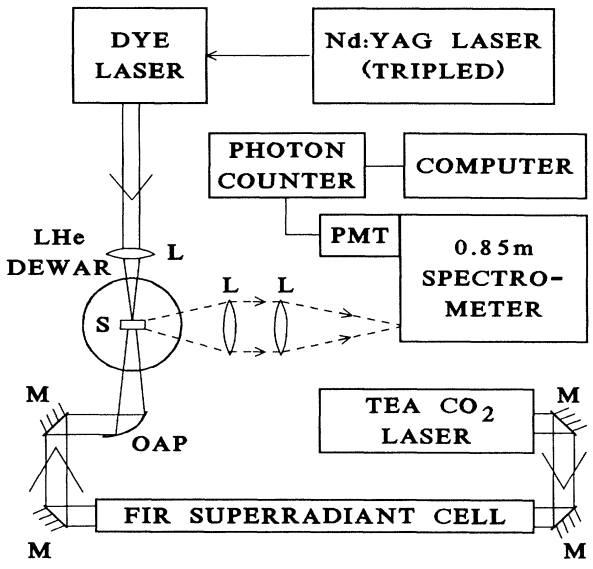

FIG. 2. Schematic of experimental setup. M: Gold coated beam steering mirrors. OAP: off-axis parabolic reflector. S: Sample. L: Delivery and collection optics. PMT: photomultiplier tube.

Using an off-axis parabolic reflector, the resulting FIR radiation was focused to a 2-mm spot size at the sample with pulse energies in the range 0.1–1 mJ. Optical detection by anti-Stokes absorption vibronic sideband spectroscopy was achieved using a Nd:YAG pumped dye laser and amplifier system which was further optically filtered using an external 1 m spectrometer. The sample was immersed in a 1.8-K liquid helium bath. The FIR and optical beams were incident on the sample in a counterpropagating geometry, with the phonon-induced fluorescence detected at 90 degrees to the pump beams. This fluorescence was spectrally filtered using an 0.85-m double monochromator. The time-integerated signal was detected using standard gated photon-counting techniques. It should be noted that in the presence of high-occupation-number phonon distributions, the phonon-induced fluorescence could be detected by eye and was observed to originate from the whole interaction region demonstrating that bulk phonons were indeed being generated.

RESULTS AND DISCUSSION

Figure 3 shows the phonon spectra after monochromatic phonon generation at $\nu_g=51.9$ cm^{-1}. The first trace, which was taken at a delay of 21 ns after the beginning of the FIR pulse, exhibits a distinct monochromatic peak at the generation frequency characteristic of DIOPA. We note that the spectral resolution is limited by the optical detection scheme to be ~ 0.5 cm^{-1}, as described above. The true width of this phonon distribution should be of the order of the FIR pump laser (<0.02 cm^{-1}). The actual occupation number of this peak is thus greater than that shown by the ratio of the detection to generation widths. The feature below 30 cm^{-1} in this trace shows the noise associated with ν^2 roll-off in sensitivity with frequency due to the Debye density of states.

At later times (77 ns), the monochromatic peak has nearly decayed with two distinct broadband features dominating the spectrum. The low-frequency phonon band below 30 cm^{-1} has increased in occupation number significantly above the noise level observed in the trace above and is consistent with anharmonic decay products of the 51.9-cm^{-1} phonons. We delay the discussion of the origin of the broad feature at higher phonon frequency. At still later times (133 ns) the monochromatic peak has completely decayed and the two broad features have merged together. We note however that the phonon distribution still deviates from a Planck distribution at higher frequencies.

In Fig. 4 we show a similar set of time-resolved spectra obtained after monochromatic phonon generation at 34.7 cm^{-1}. The phonon spectra exhibit similar features to those observed for the 51.9-cm^{-1} case. From this data we note that the broad frequency band which lies at higher frequencies is centered on the generation frequen-

cy and builds up more rapidly than the lower frequency band. The inset in Fig. 4(a) shows the presence of a narrow peak at twice the generation frequency. We attribute this feature to the confluence of two 34.7-cm^{-1} phonons which are generated with occupation numbers greater than one. The presence of this band at twice ν_g enables us to attribute the broadband feature which occurs centered on ν_g to the decay products of the $2\nu_g$ distribution.

The phonon spectra obtained several microseconds after the FIR pumping at both 34.7 and 51.9 cm^{-1} are shown in Fig. 5. The smooth curves show Planck distributions at temperatures of 10 and 9 K, respectively, demonstrating that within our detection range the phonons have nearly reached thermal equilibrium.

RATE EQUATION MODEL

We analyze this data by comparing it to the solutions of a set of occupation-number rate equations which take into account the following processes. Anharmonic decay to broadband phonon distributions centered at half the frequency of the parent phonons; phonon confluence of narrow band phonons to a similarly narrow band at twice the parent frequency; and broadband backfeeding processes. The pertinent phonon distributions and the interactions between them are represented schematically using the set of six levels in Fig. 6. Level 2 represents a narrow-band phonon distribution of width 500 MHz at the generation frequency ν_g. Level 1 represents a second narrow-band phonon distribution at $2\nu_g$ which is populated by confluence of two phonons of frequency ν_g. These two distributions are used as source terms to populate a set of four broadband distributions at $2\nu_g$, ν_g, $\nu_g/2$, and $\nu_g/4$ denoted by levels 3–6, respectively. Recombination from the decay products of the $\nu_g/4$ phonons was not included as the time scale for these processes was greater than that of the experimental results. In order to consider the interactions between the narrow-

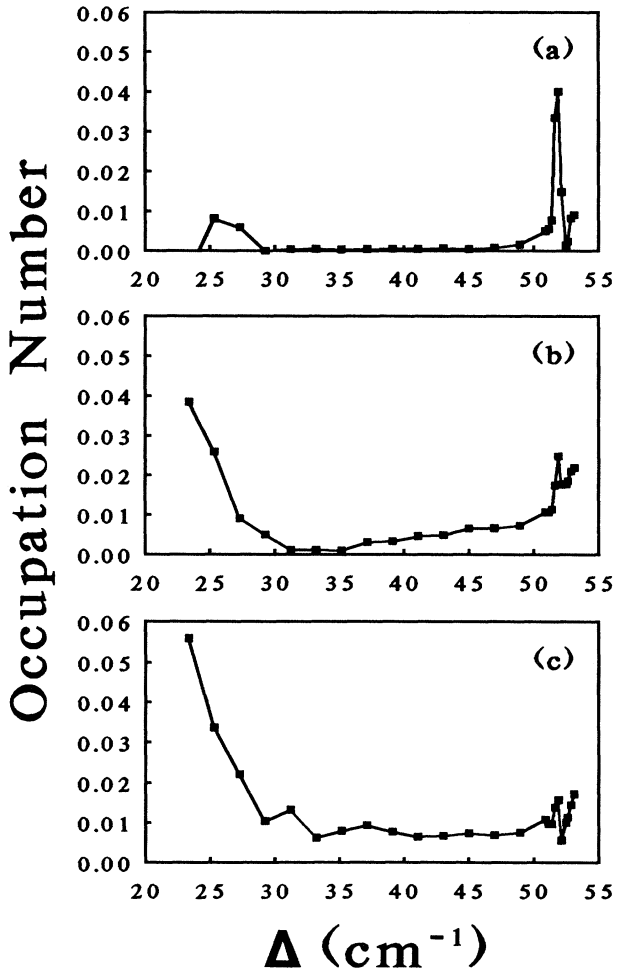

FIG. 3. Phonon spectral distributions following FIR phonon generation at 51.9 cm^{-1} for several delays (t_d). (a) $t_d=21$ ns, (b) $t_d=77$ ns, (c) $t_d=133$ ns. The solid lines connecting the data points are added as guides to the eye.

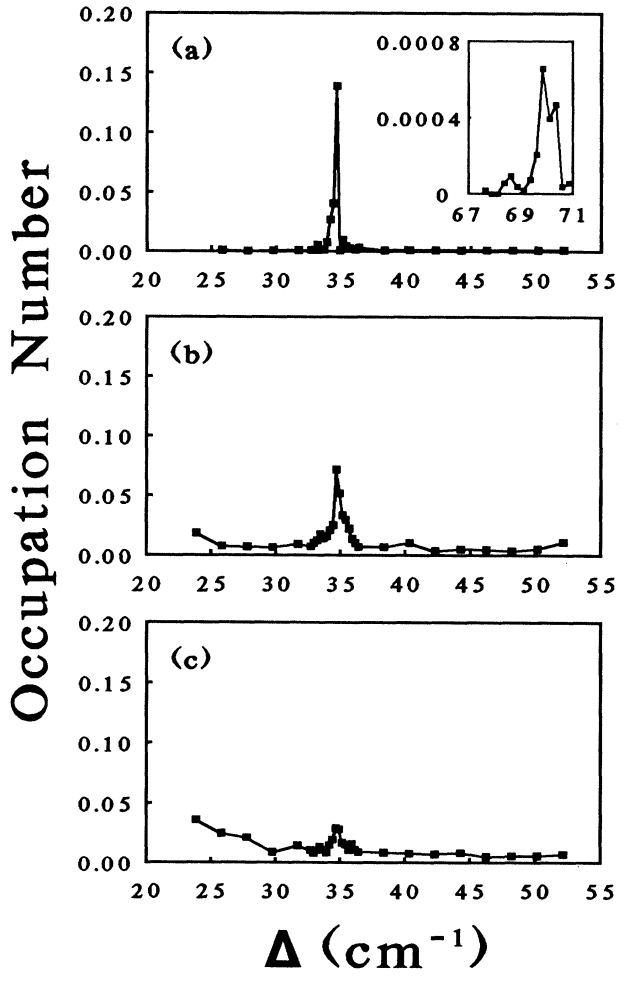

FIG. 4. Phonon spectral distributions following FIR phonon generation at 34.7 cm^{-1} for several delays (t_d). (a) $t_d=35$ ns. The spectrum at $2\nu_g=69.4$ cm^{-1} is shown in the inset. (b) $t_d=91$ ns, (c) $t_d=147$ ns. The solid lines connecting the data points are added as guides to the eye.

band phonon distributions generated by DIOPA and the broadband distributions generated as a result of anharmonic decay, we model the broadband distributions by a representative set Einstein modes with a frequency width of the FIR laser pulse δ_{FIR} using the formalism of Schaich.[8]

Our model is based on the following assumptions.

(i) Anharmonic decay rates can be scaled by ν^5 according to the isotropic dispersionless model.[9]

(ii) The phonon distribution which is generated as a result of anharmonic decay is centered at half the frequency of the parent distribution and has a width proportional to the center frequency.

(iii) The narrow-band phonon distributions at ν_g and $2\nu_g$ have the frequency width of the FIR laser.

(iv) Elastic scattering processes are sufficiently fast that phonons do not escape the interaction volume on the time scale of the experiment.

(v) All phonons lie on the same branch.

The occupation-number rate equations describing this system can be written

$$\frac{dn_1}{dt} = -W_1^- n_1(n_4+1)^2 - w_1^-[n_1(n_2+1)^2-(n_1+1)n_2^2] , \tag{3a}$$

$$\frac{dn_2}{dt} = P(t) - W_2^- n_2(n_5+1)^2 + 8w_2^+[n_1(n_2+1)^2-(n_1+1)n_2^2] , \tag{3b}$$

$$\frac{dn_3}{dt} = -W_3^-[n_3(n_4+1)^2-(n_3+1)n_4^2] , \tag{3c}$$

$$\frac{dn_4}{dt} = -W_4^-[n_4(n_5+1)^2-(n_4+1)n_5^2] + 16W_4^+[n_3(n_4+1)^2-(n_3+1)n_4^2] + 8w_4^+ n_1(n_4+1)^2 , \tag{3d}$$

$$\frac{dn_5}{dt} = -W_5^-[n_5(n_6+1)^2-(n_5+1)n_6^2] + 16W_5^+[n_4(n_5+1)^2-(n_4+1)n_5^2] + 8w_5^+ n_2(n_5+1)^2 , \tag{3e}$$

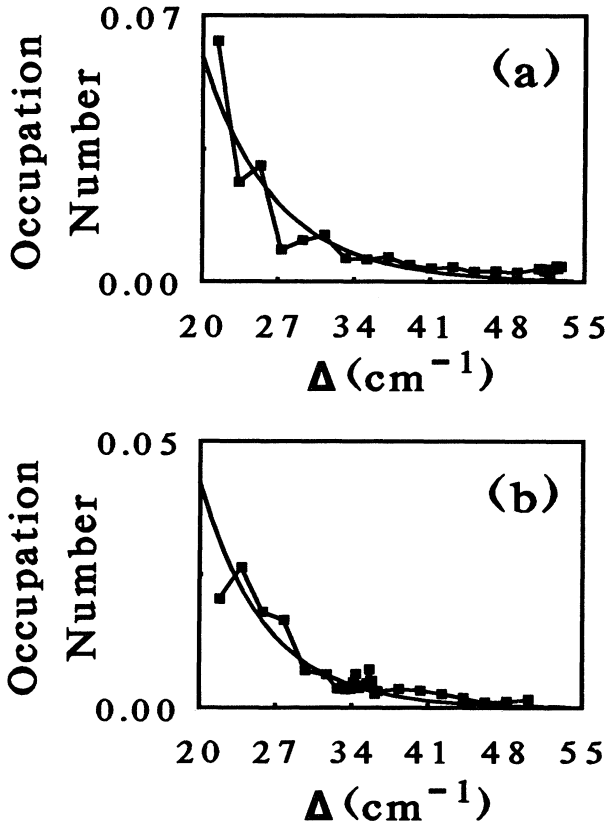

FIG. 5. Phonon spectral distributions observed at long delays after phonon generation demonstrating the establishment of quasiequilibrium. The solid lines show the Planck distributions that best fit the data. (a) Spectrum at 4.8-μs delay following generation at 51.9 cm^{-1}. Thermal distribution at $T=10$ K. (b) Spectrum at 3.2-μs delay following generation at 34.7 cm^{-1}. Thermal distribution at $T=9$ K.

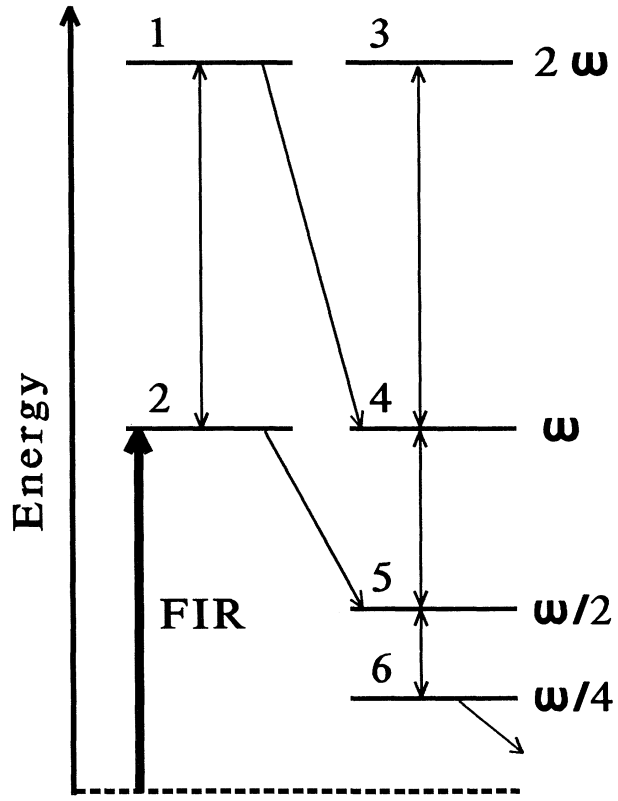

FIG. 6. Energy level schematic depicting the interaction between narrow-band phonon distributions at $2\nu_g$ and ν_g (levels 1 and 2), and the set of Einstein modes (levels 3–6). The heavy vertical arrow labeled FIR represents the monochromatic phonon generation by defect-induced one-phonon absorption.

$$\frac{dn_6}{dt} = -W_6^- n_6 + 16W_6^+ [n_5(n_6+1)^2 - (n_5+1)n_6^2] , \tag{3f}$$

where $P(t)$ is a Gaussian source term that represents the FIR pumping of defect-induced one-phonon absorption at ν_g. The rates W_i^- are calculated from the inverse of the anharmonic decay time for phonons of frequency ν_i. It should be noted that $\nu_1=\nu_3$ and $\nu_2=\nu_4$, which implies $W_1^- = W_3^-$ and $W_2^- = W_4^-$ and also that $W_i^- = W_{i+1}^+$ for $i=1-2$ and $3-6$. The rates $w_i^- = (\delta_{\rm FIR}/\delta_{i+1})W_i^- = w_{i+1}^+$ arise as a result of energy conservation in order to take into account the difference in width between the narrow-band phonon distributions at ν_g and $2\nu_g$ (ν_1 and ν_2) and the broadband phonon distributions at ν_i ($i=3-6$). For the case of FIR pumping at 34.7 cm^{-1}, the adjustable parameters for the model which provided the best agreement with the data were a peak pump rate of $P(0)=4\times10^8$ s^{-1} and an anharmonic decay rate of $W_2^- = 2.5\times10^7$ s^{-1} for the 34.7 cm^{-1} phonons. All other rates were obtained by scaling W_2^- by ν^5 according to the isotropic dispersionless model. The widths δ_i of the broadband distributions were taken to be 50% of the center frequency ν_i for all calculations.

In Fig. 7 we present a comparison of the experimental data taken at 34.7 cm^{-1} with the results of the model described above. On the left are phonon transients at 69.4 cm^{-1} ($2\nu_g$), 34.7 cm^{-1} (ν_g), and 35.7 cm^{-1} (ν_g+1) cm^{-1}, respectively, while the smooth curves on the right show the results of the model calculations for phonon distributions at the same frequencies. The calculated transients at $2\nu_g$ and ν_g are constructed from weighted sums of the broad- and narrow-band distributions at those frequencies, for comparison with experimental data. For example, the observed occupation number $n_{\rm obs}$ at frequency ν_g is calculated using

$$n_{\rm obs} = \left[\frac{\delta_{\rm gen}}{\delta_{\rm det}}\right] n_2 + n_4 , \tag{4}$$

where $\delta_{\rm gen}$ and $\delta_{\rm det}$ are the bandwidths of generation and detection, respectively.

The transient at (ν_g+1) cm^{-1} is representative of the broadband distribution centered at ν_g. The rise time of this distribution was strongly dependent on the presence of the feeding mechanism involving the generation of phonons at $2\nu_g$. A substantially poorer agreement between the model and the experimental data was obtained if the rate w_1^- was set to zero.

A comparison of the experimental data with the model for FIR pumping at 31.2 and 43.3 cm^{-1} showed similar agreement.[10] In the case of the 43.3-cm^{-1} pumping it was necessary to increase the rate w_1^- by a factor 6 in order to obtain good agreement with the experimental data. We note that this is consistent with the high density of phonon states at the generation frequency due to the presence of a low-lying optical mode in this system.[11] The only other parameters adjusted in both cases were the FIR pump power and the anharmonic decay times of the resonant phonons.

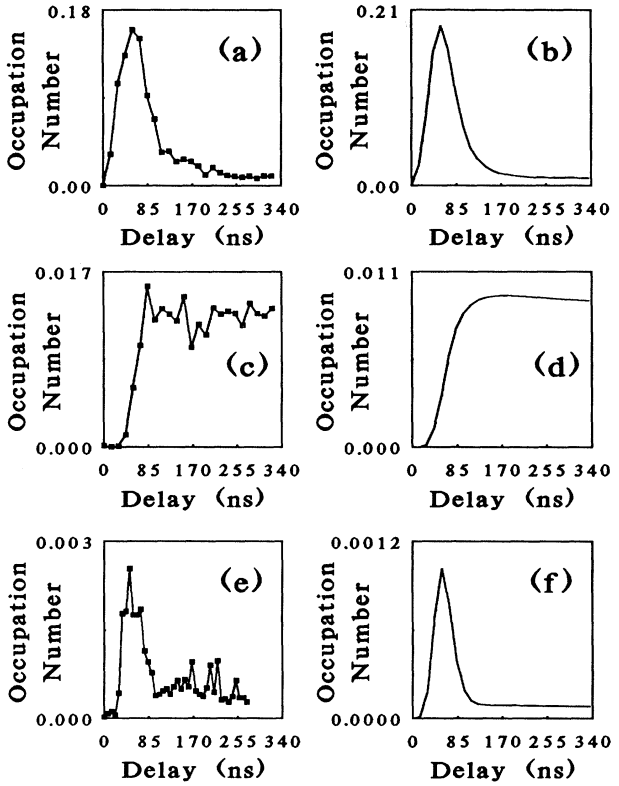

FIG. 7. Comparison of experimentally observed data with numerical solutions of rate equations for 34.7 cm^{-1} phonon generation. (a) Experimental resonant transient at $\nu_g=34.7$ cm^{-1}. (b) Resonant transient calculated from Eq. (4). (c) Experimental nonresonant transient (35.7 cm^{-1}). (d) Nonresonant transient (n_4). (e) Experimental transient at $2\nu_g=69.4$ cm^{-1}. (f) Transient calculated from n_1, n_3, and Eq. (4).

In light of the simplifying assumptions described above, we feel that the overall agreement, both qualitative and quantitative, between the model and the experimental data is very good. The most severe assumption, that of a single branch model and hence the elimination of mode conversion considerations would appear to preclude obtaining quantitative agreement between model and experiment. We note that if momentum conservation is relaxed for anharmonic decay processes as well as for DIOPA then the one-branch model would provide a suitable description for this system.[12]

CONCLUSIONS

Defect-induced one-phonon absorption has been used to generate monochromatic phonon distributions for phonon spectroscopy in $LaF_3:Pr^{3+}$. The spectral dynamics associated with high-occupation number narrow-band phonon distributions at 34.7 and 51.9 cm^{-1} have been investigated over the frequency range between 30 and 55 cm^{-1}. The path to equilibrium in both cases appears to involve both anharmonic decay and upconversion. At intermediate time scales, two distinct broadband distribu-

tions have been observed. These are attributed to direct anharmonic decay processes and the anharmonic decay of a second narrow-band distribution at twice the generation frequency. This double frequency distribution was observed in the case of 34.7-cm^{-1} phonons and was attributed to the confluence of two phonons at the generation frequency. Comparison of the data with an occupation-number rate-equation analysis showed both qualitative and quantitative agreement. For the case of both 34.7- and 51.9-cm^{-1} phonons the spectral distributions converge on a Planckian distribution at a temperature of ~ 10 K on a microsecond time scale.

ACKNOWLEDGMENTS

This work was supported by National Science Foundation Grants DMR 8717696 and DMR 8914955.

*Current address, School of Chemical Sciences, University of Illinois at Urbana Champaign, Urbana, IL 61801.

[1]See, for example, *Nonequilibrium Phonon Dynamics—1984,* Vol. 124 of *NATO Advanced Study Institute, Series B: Physics,* edited by W. E. Bron (Plenum, New York, 1985), and references cited therein.

[2]W. A. Tolbert, W. M. Dennis, and W. M. Yen, Phys. Rev. Lett. **65**, 607 (1990).

[3]P. G. Dawber and R. J. Elliott, Proc. R. Soc. London **273**, 222 (1963).

[4]R. Orbach, Phys. Rev. Lett. **16**, 15 (1966).

[5]R. S. Meltzer, J. E. Rives, and G. S. Dixon, Phys. Rev. B **28**, 4786 (1983).

[6]W. M. Yen, W. C. Scott, and A. L. Schawlow, Phys. Rev. **136**, A271 (1964).

[7]C. T. Gross, J. Kiess, A. Mayer, and F. Keilmann, IEEE J. Quantum Electron. **2**, 377 (1987).

[8]W. L. Schaich, Solid State Commun. **49**, 55 (1984).

[9]R. Orbach and L. A. Vredevoe, Physics **1**, 91 (1964).

[10]W. A. Tolbert, Ph.D. Dissertation, University of Wisconsin-Madison, 1990 (unpublished).

[11]G. S. Dixon and R. M. Nicklow, Solid State Commun. **47**, 877 (1983).

[12]A relaxation of wave-vector conservation has recently been found necessary in the explanation of stimulated phonon emission in this material, J. E. Rives (private communication).